



This is a repository copy of *Role of carbonates in the chemical evolution of sodium carbonate-activated slag binders*.

White Rose Research Online URL for this paper:
<http://eprints.whiterose.ac.uk/100038/>

Version: Accepted Version

Article:

Bernal, S.A., Provis, J.L. orcid.org/0000-0003-3372-8922, Myers, R.J. et al. (2 more authors) (2015) Role of carbonates in the chemical evolution of sodium carbonate-activated slag binders. *Materials and Structures*, 48 (3). pp. 517-529. ISSN 1359-5997

<https://doi.org/10.1617/s11527-014-0412-6>

Reuse

Unless indicated otherwise, fulltext items are protected by copyright with all rights reserved. The copyright exception in section 29 of the Copyright, Designs and Patents Act 1988 allows the making of a single copy solely for the purpose of non-commercial research or private study within the limits of fair dealing. The publisher or other rights-holder may allow further reproduction and re-use of this version - refer to the White Rose Research Online record for this item. Where records identify the publisher as the copyright holder, users can verify any specific terms of use on the publisher's website.

Takedown

If you consider content in White Rose Research Online to be in breach of UK law, please notify us by emailing eprints@whiterose.ac.uk including the URL of the record and the reason for the withdrawal request.



eprints@whiterose.ac.uk
<https://eprints.whiterose.ac.uk/>

1 **Role of carbonates in the chemical evolution of sodium carbonate-activated slag binders**

2
3 Susan A. Bernal,¹ John L. Provis,^{1*} Rupert J. Myers,¹ Rackel San Nicolas,²
4 Jannie S.J. van Deventer^{2,3}

5
6 ¹*Department of Materials Science and Engineering, The University of Sheffield, Sheffield S1 3JD, UK*

7 ²*Department of Chemical & Biomolecular Engineering, The University of Melbourne, Victoria 3010,*
8 *Australia*

9 ³*Zeobond Pty Ltd, P.O. Box 210, Somerton, Victoria 3062, Australia*

10
11 *To whom correspondence should be addressed. Email j.provis@sheffield.ac.uk, phone +44 114 222
12 5490, fax +44 114 222 5493

13 14 **Abstract**

15
16 Multi-technique characterisation of sodium carbonate-activated blast furnace slag binders was
17 conducted in order to determine the influence of the carbonate groups on the structural and
18 chemical evolution of these materials. At early age (<4 days) there is a preferential reaction of
19 Ca²⁺ with the CO₃²⁻ from the activator, forming calcium carbonates and gaylussite, while the
20 aluminosilicate component of the slag reacts separately with the sodium from the activator to
21 form zeolite NaA. These phases do not give the high degree of cohesion necessary for
22 development of high early mechanical strength, and the reaction is relatively gradual due to the
23 slow dissolution of the slag under the moderate pH conditions introduced by the Na₂CO₃ as
24 activator. Once the CO₃²⁻ is exhausted, the activation reaction proceeds in similar way to an
25 NaOH-activated slag binder, forming the typical binder phases calcium aluminium silicate
26 hydrate and hydrotalcite, along with Ca-heulandite as a further (Ca,Al)-rich product. This is
27 consistent with a significant gain in compressive strength and reduced porosity observed after
28 3 days of curing. The high mechanical strength and reduced permeability developed in these
29 materials beyond 4 days of curing elucidate that Na₂CO₃-activated slag can develop desirable
30 properties for use as a building materials, although the slow early strength development is likely
31 to be an issue in some applications. These results suggest that the inclusion of additions which
32 could control the preferential consumption of Ca²⁺ by the CO₃²⁻ might accelerate the reaction
33 kinetics of Na₂CO₃-activated slag at early times of curing, enhancing the use of these materials
34 in engineering applications.

35 **Keywords:** alkali-activated slag; sodium carbonate; X-ray diffraction; nuclear magnetic
36 resonance; X-ray microtomography.

37

38 **1. Introduction**

39

40 Alkali-activated binders have been developed for over a century as a means for valorising
41 industrial wastes and by-products, and to produce Portland clinker free cement-like materials
42 to mitigate the environmental footprint associated with Portland cement manufacture [1, 2].
43 The production of alkali-activated binders offers a reduced embodied energy and significantly
44 lower release of pollutant gases when compared with Portland cement, and these materials can
45 develop comparable mechanical strength and performance when properly formulated and cured
46 [3, 4]. The need to develop low-cost and low-environmental footprint alkali activated materials
47 has motivated the identification and adoption of alkaline activators that can promote the
48 development of high mechanical strength and reduced permeability in the binder, and achieve
49 alkalinities comparable to those in Portland cement based materials, so that the metallic
50 component of structural concrete is not excessively corroded during the service life.

51

52 The microstructure, and therefore the performance, of alkali-activated slag materials is strongly
53 dependent on factors such as the chemistry and mineralogy of the slag precursor, the type and
54 concentration of the alkali-activator and the curing conditions [5-10]. The commonly used
55 activators for the production of activated slag binders are sodium hydroxide (NaOH), sodium
56 silicates ($\text{Na}_2\text{O} \cdot r\text{SiO}_2$), sodium carbonate (Na_2CO_3) and sodium sulfate (Na_2SO_4) [6, 9, 11, 12].
57 It is well known that the effectiveness of the activator is based on its ability to generate an
58 elevated pH, as this controls the initial dissolution of the precursor and the consequent
59 condensation reaction to form the reaction products [13-15].

60

61 A high pH is expected to favour the dissolution of the slag to form strength-giving phases such
62 as calcium aluminium silicate hydrate (C-A-S-H) type gels [16]. However, pH is not the only
63 factor controlling the mechanism of reaction taking place when activating slag. It has been
64 observed [17, 18] that using a sodium silicate activator, which has a lower pH than sodium
65 hydroxide solutions, when dosed with equivalent Na_2O content, promotes the development of
66 binders with higher mechanical strength. This is a consequence of the additional silicate species
67 that it provides to the system, and the interparticle electrostatic forces governing the formation
68 of the binder when using this activator [19]. This indicates that the functional group

69 accompanying the alkaline activator is playing an important role in the activation mechanism
70 of these materials.

71

72 Sodium carbonate activation of blast furnace slag has been applied for half a century in Easter
73 Europe [20, 21], as a lower cost and more environmentally friendly alternative to the widely
74 used activators sodium hydroxide or sodium silicate used for production of activated slag
75 products [22, 23]. More recent work on Na_2CO_3 -slag-fine limestone concretes showed very
76 good early strength development, and calculated potential Greenhouse emission savings as
77 high as 97% compared to Portland cement [24-26]. The use of this activator forms binders with
78 reduced pH compared with materials produced with NaOH and $\text{Na}_2\text{O}\cdot r\text{SiO}_2$ [27]. This is
79 especially attractive for specialized applications such as the immobilisation of nuclear wastes
80 containing reactive metals which corrode at high pH [27]. However, the understanding of the
81 structural development of carbonate-activated slag is very limited, as carbonate-activated
82 binders have attracted less attention than other activated-slag systems because of the delayed
83 hardening (which can take up to 5 days in some systems) and slower strength development [28-
84 30], when compared with other alkali-activated slag binders.

85

86 It has been identified [26, 29] that at early times of reaction of Na_2CO_3 -activated slags form
87 calcium and mixed sodium-calcium carbonates, as a consequence of the interaction of the CO_3^{2-}
88 from the activator with the Ca^{2+} from the dissolved slag; however, longer times of curing favour
89 the formation of C-A-S-H type gels. Xu et al. [21] evaluated aged slag activated with Na_2CO_3
90 and $\text{Na}_2\text{CO}_3/\text{NaOH}$ blends, and identified as the main reaction product a highly crosslinked C-
91 A-S-H type phase with a reduced content of Ca in the outer product, along with an inner product
92 involving carbonate anions. Formation of Ca-Na mixed carbonates was not detected in aged
93 Na_2CO_3 -activated slag concretes, which differs from what has been identified in young (28-
94 day) samples where gaylussite is often observed [26, 31].

95

96 It has been proposed [21] that in Na_2CO_3 activated slag binders the activation reaction takes
97 place through a cyclic hydration process where the Na_2CO_3 supplies a buffered alkaline
98 environment where the level of CO_3^{2-} available in the system is maintained by the continual
99 dissolution of CaCO_3 in equilibrium with the pore solution, releasing Ca^{2+} to react with the
100 dissolved silicate from the slag to form C-S-H type products. However, there is not yet detailed
101 evidence of how this mechanism might be established and then proceed over the first months
102 of reaction in Na_2CO_3 -activated slags.

103

104 In this study the structural evolution of sodium carbonate activated slag pastes is assessed
105 through X-ray diffraction, ^{29}Si and ^{27}Al MAS NMR spectroscopy and X-ray microtomography.
106 Isothermal calorimetry of fresh paste is also conducted in order to determine the kinetic of
107 reaction of sodium carbonate pastes. Compressive strength values of mortars corresponding to
108 the pastes produced for the structural study are reported in order to develop a better
109 understanding of the relationship between the structural characteristics of these binders and
110 their mechanical strength development.

111

112

113 2. Experimental program

114

115 2.1. Materials and sample preparation

116 As primary raw material a granulated blast furnace slag (GBFS) was used, supplied by Zeobond
117 Pty Ltd., Australia, with oxide composition as shown in Table 1. Its specific gravity is 2800
118 kg/m^3 and Blaine fineness $410 \pm 10 \text{ m}^2/\text{kg}$. The particle size range, determined through laser
119 granulometry, was 0.1-74 μm , with a d_{50} of 15 μm .

120

121 **Table 1.** Composition of GBFS used. LOI is loss on ignition at 1000°C

Component (mass % as oxide)	GBFS
SiO_2	33.8
Al_2O_3	13.7
Fe_2O_3	0.4
CaO	42.6
MgO	5.3
Na_2O	0.1
K_2O	0.4
Others	1.9
LOI	1.8

122

123 Commercial sodium carbonate (Sigma-Aldrich) was dissolved in the mix water until complete
124 dissolution was reached. The assessment of structural evolution was conducted in paste
125 specimens formulated with a water/binder ratio of 0.40 and an activator (Na_2CO_3) content of 8

126 wt.% relative to the amount of slag for strength development, NMR, XRD and calorimetry
127 analysis, and 7 wt.% for microtomography. All paste specimens were cured in sealed centrifuge
128 tubes at 23°C until testing. Mortar cubes, 50 mm in size, were used for compressive strength
129 testing; these were formulated with a sand:binder ratio of 2:75, and a binder formulation
130 matching the paste specimens.

131

132 Isothermal calorimetry experiments were conducted using a TAM Air isothermal calorimeter,
133 at a base temperature of $25 \pm 0.02^\circ\text{C}$. Fresh paste was mixed externally, weighed into an
134 ampoule, and immediately placed in the calorimeter, and the heat flow was recorded for the
135 first 140 h of reaction. All values of heat release rate are normalised by total weight of paste.

136

137 **2.2. Tests conducted on hardened specimens**

138 The hardened paste specimens were analysed after periods of up to 45 days of curing through:

139

- 140 • Compressive strength testing, using an ELE International Universal Tester, at a loading
141 rate of 1.0 kN/s for the 50 mm mortar cubes.
- 142 • X-ray diffraction (XRD), using a Bruker D8 Advance instrument with Cu K α radiation
143 and a nickel filter. The tests were conducted with a step size of 0.020° , over a 2θ range of
144 5° to 70° .
- 145 • Magic angle spinning nuclear magnetic resonance (MAS NMR) spectroscopy; ^{29}Si MAS
146 NMR spectra were collected at 119.1 MHz on a Varian INOVA-600 (14.1 T) spectrometer
147 using a probe for 4 mm o.d. zirconia rotors and a spinning speed of 10.0 kHz. The ^{29}Si
148 MAS experiments employed a pulse width of 6 μs , a relaxation delay of 60 s and 4300-
149 6500 scans. Solid-state ^{27}Al MAS NMR spectra were acquired at 156.3 MHz on the same
150 instrument, with a pulse width of 6 μs , a relaxation delay of 2 s. All the spectra were
151 collected with a pulse angle of 51° . ^{29}Si and ^{27}Al chemical shifts are referenced to external
152 samples of tetramethylsilane (TMS) and a 1.0 M aqueous solution of $\text{AlCl}_3 \cdot 6\text{H}_2\text{O}$,
153 respectively.
- 154 • Samples cured for up to 45 days and ~ 1 mm in size were analysed using beamline 2-BM
155 at the Advanced Photon Source, Argonne National Laboratory [32]. Reactions were halted
156 after the specified curing duration by immersion of the samples in acetone until testing,
157 and analytical specimens were taken from the part of the sample close to the interface
158 between solid material and acetone to ensure that the reaction had been halted promptly in

159 the sections use for testing. Measurements were carried out using hard X-ray synchrotron
160 radiation (22.5 keV) in a parallel-beam configuration, with 0.12° rotation per step (1501
161 steps in a 180° rotation) and 0.4 s exposure time per step. Samples were mounted in small
162 polymeric cones to enable alignment; sample size and shape were somewhat irregular, as
163 the samples were obtained by fracturing larger monoliths, but all samples fitted within the
164 field of view in the horizontal plane of the detector. X-ray detection was achieved with a
165 scintillator and CCD camera, capturing 2048×2048 pixels. Tomographic data were
166 reconstructed using an in-house developed reconstruction algorithm, including recentring
167 following visual inspection to ensure optimal reconstructions, using a voxel size of 0.75
168 µm (corresponding to the detector resolution). The segmentation, pore connectivity and
169 tortuosity calculations on volume of interest (VOI) regions of at least 400 pixels³ were
170 performed following the protocol described in [33].

171

172

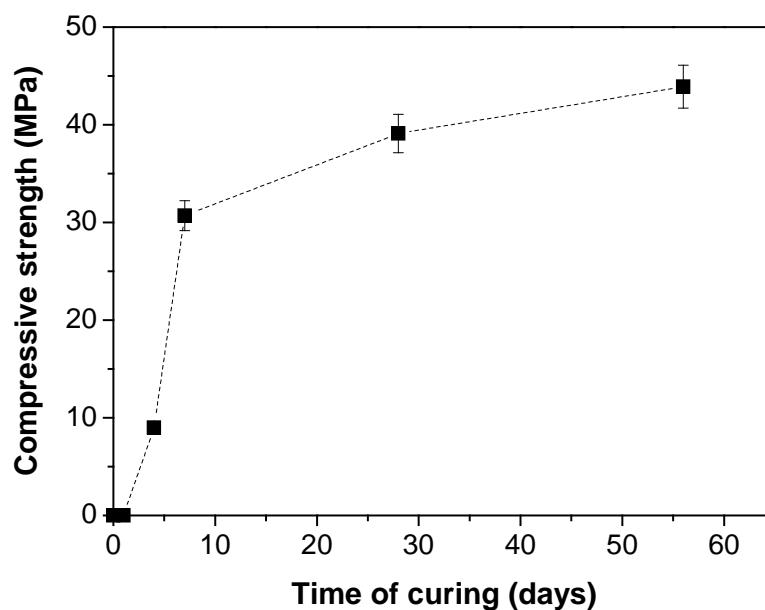
173 **3. Results and discussion**

174

175 **3.1. Compressive strength**

176 The compressive strength of sodium carbonate activated slag mortars could not be determined
177 at 1 day because the material was still soft. However, after 4 days the mortars gained a
178 compressive strength of 9 MPa (Figure 1), followed by a substantial rise in the subsequent 3
179 days to reach 31 MPa after 7 days of curing. This compressive strength gain indicates that the
180 initial mechanism of reaction in sodium carbonate activated slag binders is not leading to the
181 formation of strength-giving phases during the first days of curing, and consequently the
182 samples are not developing a measurable compressive strength during this time. Subsequently,
183 there is an increase in the formation of strength-giving phases from 4 to 7 days, with an
184 associated jump in strength. After this, there is an ongoing gradual increase in the compressive
185 strength with extended curing (up to 44 MPa at 56 days).

186



187

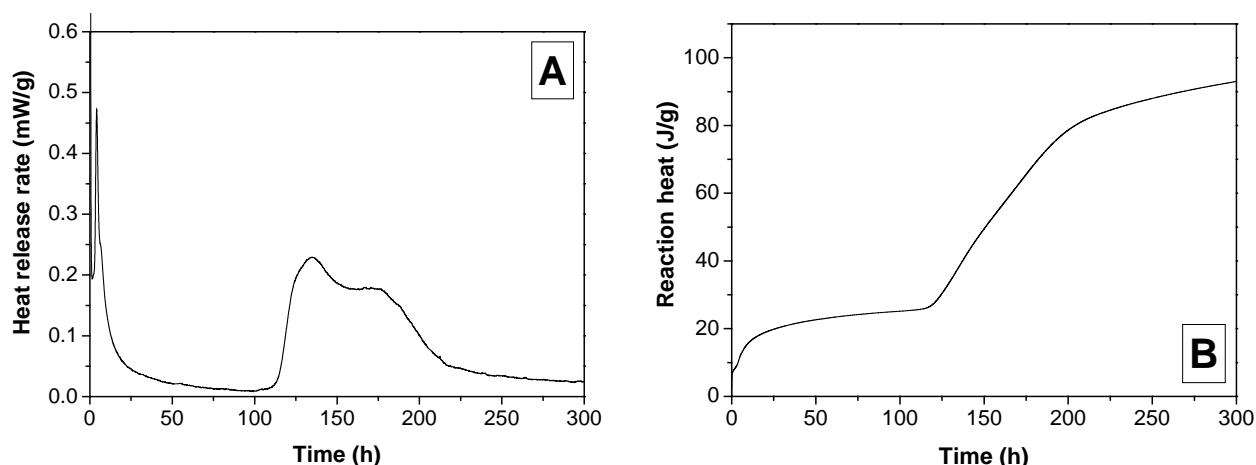
188 **Figure 1.** Compressive strength of sodium carbonate-activated slag binders as a function of
189 the time of curing

190

191 3.2. Isothermal calorimetry

192 The heat release curves of the sodium carbonate activated slag are shown in Figure 2. There is
193 an initial pre-induction period, associated with the partial dissolution of the slag particles, in
194 the first 48 h, followed by an extended induction period (~62 h) where little heat evolution is
195 taking place. This is consistent with the fact that hardening is observed to take place slowly
196 during the first 4 days of curing in these samples. Extended induction periods in sodium
197 carbonate activated slag binders have also been observed by Fernandez-Jimenez et al. [34];
198 however, in that study the precipitation of reaction products was observed via an acceleration
199 in heat release 6 hours after mixing, rather than after several days here. The differences in the
200 results between studies can be mainly attributed to the differences in the chemistry of the slag
201 (mainly the MgO content), as the specific surface and amorphous content of the material used
202 in that work seem to be similar to the slag used in the present study. The MgO content of slag
203 has recently been identified to play a key role in defining the nature of the reaction products in
204 alkali-activated slag binders [35], and this is the main identifiable difference between the two
205 binder systems.

206



207 **Figure 2.** (A) Heat release rate and (B) cumulative heat release of sodium carbonate-
208 activated slag binders

209

210 After the induction period, a high intensity heat evolution process, corresponding to the
211 processes generally described as the acceleration and deceleration periods in cementitious
212 binders (~110-220 h) is identified. This peak corresponds to the precipitation of voluminous
213 reaction products in the binder, releasing a significant heat of reaction. In this case the heat
214 release seems to be occurring in two consecutive stages, as two clear maximum heat release
215 peaks are observed in Figure 2A. The occurrence and timing of the acceleration-deceleration
216 period agree well with the increase in compressive strength observed in these specimens
217 (Figure 1) at a similar time of curing, confirming that the formation of the bulk binding phases
218 responsible for both strength and heat output is not taking place during the first 3 days of
219 reaction. This is to a significant extent consistent with the very moderate initial pH of these
220 binders, as it takes time for the pH to increase to the point where the slag will start to react
221 rapidly to form these binding phases.

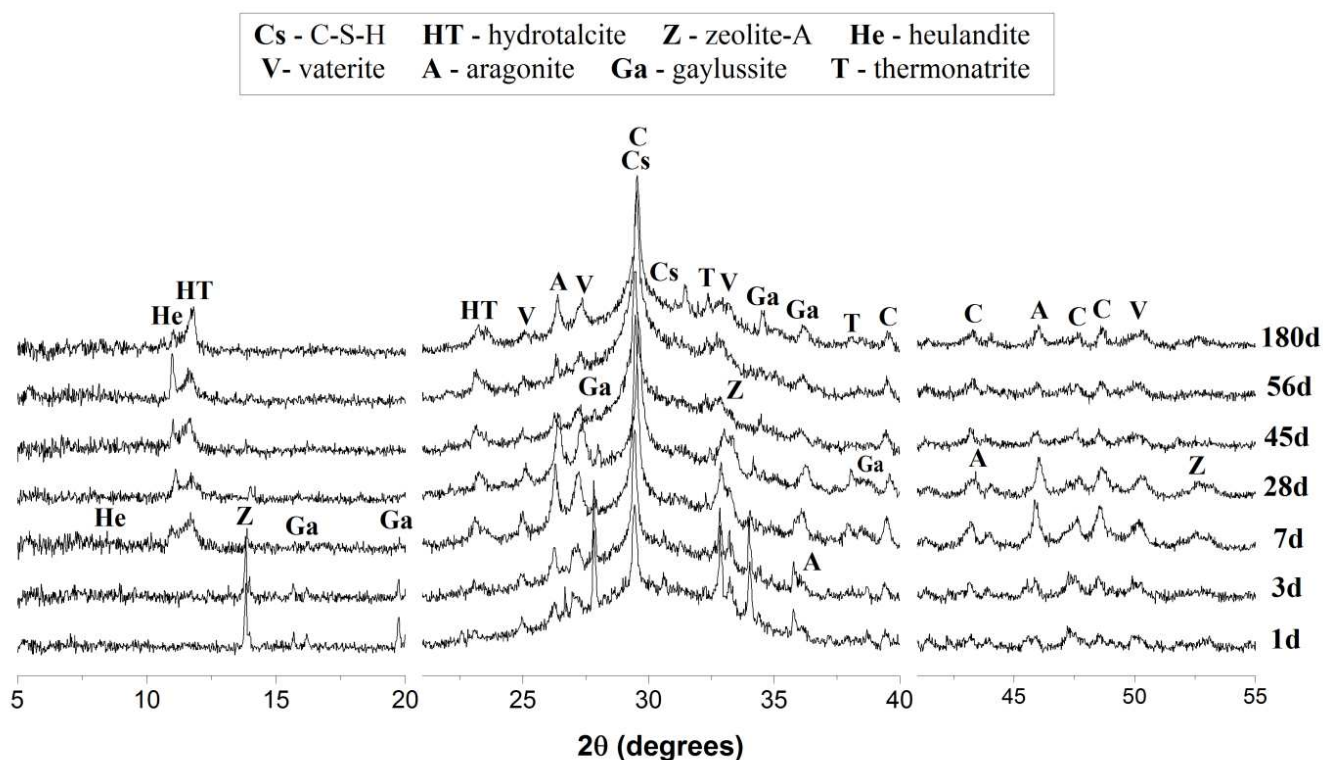
222

223 These results different from those identified in sodium silicate activation of this same slag [35],
224 and in other systems with comparable slag chemistry [18], where the pre-induction period was
225 observed during the first hours of reaction, followed by short induction periods (<10 h in
226 metasilicate activated slags with MgO contents lower than 8 wt.% [35]). However, it has been
227 noted [36], that in sodium metasilicate activation of slags with reduced alumina (11.9 wt.%)
228 content, the induction period was as long as 6 days. This elucidates that delayed precipitation
229 of reaction products is not an exclusive effect of the nature of the alkaline activator, but also
230 relates to the chemical and mineralogical composition of the slag used.

231

232 3.3. X-ray diffraction

233 The evolution of crystalline phases forming in a sodium carbonate activated slag is shown in
 234 Figure 3. In samples cured for one day the main crystalline compounds forming are the three
 235 polymorphs of calcium carbonate (CaCO_3): calcite (powder diffraction file, PDF #005-0586),
 236 vaterite (PDF #002-0261) and aragonite (PDF #04-013-9616), along with the double salt
 237 gaylussite ($\text{Na}_2\text{Ca}(\text{CO}_3)_2 \cdot 5\text{H}_2\text{O}$, PDF #021-0343) and zeolite NaA ($\text{Na}_{12}\text{Al}_2\text{Si}_{12}\text{O}_{48} \cdot 18\text{H}_2\text{O}$,
 238 PDF#039-0221). Formation of calcium carbonate in various polymorphs, and gaylussite, has
 239 been identified in carbonated alkali-activated slag binders [37, 38]. The identification of similar
 240 reaction products in the carbonate-activated binder suggests that there is a preferential early
 241 age reaction between dissolved CO_3^{2-} present in the pore solution and the Ca^{2+} released by the
 242 partial dissolution of the slag. The consumption of Ca^{2+} by CO_3^{2-} then leads to a saturation of
 243 Si and Al species with respect to aluminosilicate type products such as zeolite NaA in the
 244 NaOH-rich pore solution from the very earliest stages of the reaction process.



246 **Figure 3.** X-ray diffractograms of sodium carbonate-activated slag binders as a function of
 247 the time of curing, as shown.

248
 249 After 7 days of curing, the intensities of the zeolite NaA and gaylussite peaks have decreased;
 250 these phases are almost fully consumed by 45 days. Instead, the Ca-containing zeolite

251 heulandite (approximately $\text{CaAl}_2\text{Si}_7\text{O}_{18} \cdot n\text{H}_2\text{O}$, $n = 3.5$ to 6, PDF# 025-0144 or 024-0765) and
252 a calcium aluminium silicate hydrate (C-A-S-H) (resembling a disordered, Al-substituted form
253 of tobermorite-11Å, $\text{Ca}_5\text{Si}_6\text{O}_{18} \cdot 5\text{H}_2\text{O}$, PDF #045-1480), and a layered double hydroxide with
254 a hydrotalcite type structure ($\text{Mg}_6\text{Al}_2\text{CO}_3(\text{OH})_{16} \cdot 4\text{H}_2\text{O}$, PDF# 014-0191), are observed.
255 Heulandite has been identified as a secondary reaction product in preparation of synthetic C-
256 A-S-H phases with 30% silicon replacement by aluminium [39] and in aged (7 years) silicate-
257 activated slag binders [40], while C-A-S-H products along with hydrotalcite are the main
258 reaction products forming in alkali-activated slags produced with either NaOH or $\text{Na}_2\text{O} \cdot r\text{SiO}_2$
259 [18, 31, 37, 41]. The formation of these reaction products indicates that once the CO_3^{2-} supplied
260 by the alkaline activator is largely consumed in the formation of carbonate compounds, which
261 is likely to be the case after a few days of reaction, the mechanism of reaction of sodium-
262 carbonate activated slags proceeds in the same way as in sodium hydroxide-activated or sodium
263 silicate-activated systems. This is in good agreement with the rise in the mechanical strength
264 identified in these samples at this time.

265

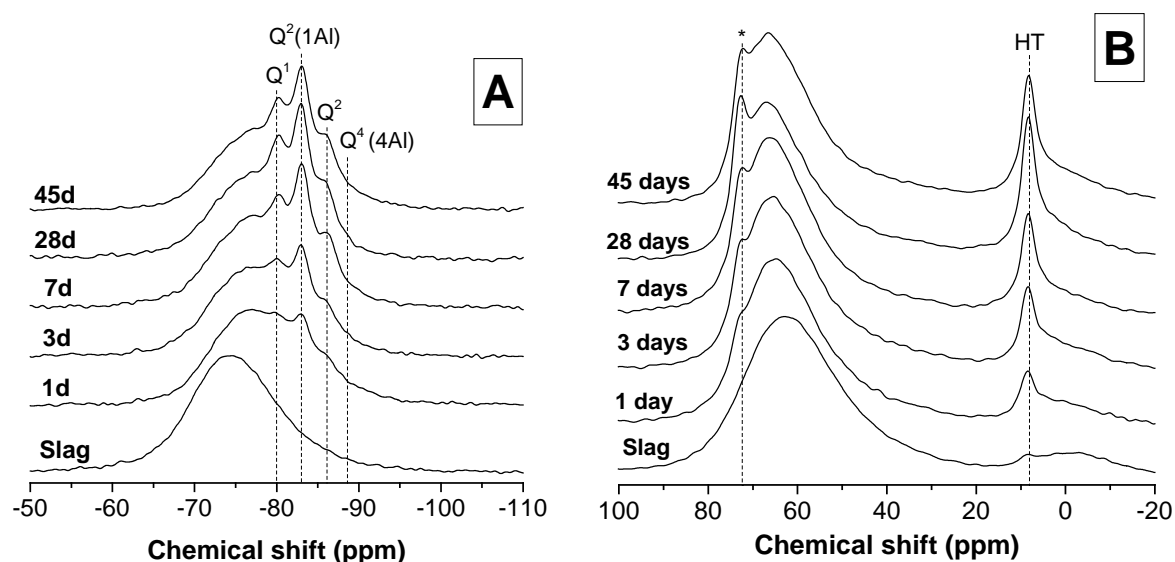
266 Traces of thermonatrite ($\text{Na}_2\text{CO}_3 \cdot \text{H}_2\text{O}$) are identified in all samples after 28 or more days of
267 curing, which suggest that this is not simply a dried remnant of the remnant activator in the
268 pore solution, as it is not observed in the younger samples. Instead, thermonatrite is likely to
269 be a product derived from the carbonation of the pore solution during exposure to ambient air
270 for XRD analysis, as it has also been identified in carbonated metasilicate-activated slags [35,
271 37, 42]. Significant increases in the intensities of the reflections assigned to heulandite,
272 hydrotalcite and C-A-S-H are observed at advanced times of curing; however, it seems that
273 after 180 days, the systems is mainly dominated by hydrotalcite and C-A-S-H, with traces of
274 sodium and calcium carbonate compounds. Gaylussite appears to have been converted entirely
275 to more stable products. An extended period of formation of these reaction products is
276 controlling the ongoing compressive strength gain observed in these binders (Figure 1).

277

278 3.4. Nuclear Magnetic Resonance

279 The ^{29}Si MAS NMR spectra of the anhydrous slag and sodium carbonate-activated binders
280 (Figure 4A) show little change after 1 day of curing, consistent with a relatively slow rate of
281 reaction of the slag. However, a low intensity peak is observed at -83 ppm, consistent with a
282 $\text{Q}^2(1\text{Al})$ site characteristic of the Al substituted C-S-H type phase which forms in alkali-
283 activated slags [35, 37, 43], which suggests that the preferential formation of carbonates is not
284 completely hindering the formation of this product. In this spectrum it is also possible to

285 identify a shoulder at -89.5 ppm which corresponds to the presence of zeolite NaA [44], which
286 becomes less prominent beyond 7 d as the prevalence of this phase decreases. There is no clear
287 peak due to heulandite observable (in the region around -100 ppm [45]) at longer ages, but the
288 concentration of this phase is always low according to XRD also.
289



290 **Figure 4.** (A) ^{29}Si and (B) ^{27}Al MAS NMR spectra of sodium carbonate-activated slag
291 binders as function of the time of curing. HT is hydroxylated talc, and the asterisk corresponds to
292 Al in Q^2 sites in the C-A-S-H phase
293
294

295 At increased times of reaction, the formation of sites at -80 ppm, -83 ppm and -86 ppm,
296 corresponding to the Q^1 , $\text{Q}^2(1\text{Al})$ and Q^2 species in C-A-S-H products [46, 47], becomes
297 increasingly clear. A higher intensity of these sites is observed with increasing curing time,
298 consistent with the higher intensity of the C-A-S-H phase reflections identified by XRD (Figure
299 3), and the increased strength of the binders over the time of curing (Figure 1). Complicating
300 any quantitative analysis of these spectra is an apparently partially-selective reaction of the
301 slag, which means that direct subtraction of an unreacted component from the spectra – which
302 is a prerequisite for any useful deconvolution – is unfortunately not possible. This partial
303 selectivity is evident from observation of the region around -65 to -70 ppm in Figure 4A, where
304 the signal in this region corresponds to the highly depolymerised (Q^0) silicate component
305 within the slag glass. Because these sites in the slag are able to be released without the need to
306 break any of the relatively strong Si-O-Al or Si-O-Si network bonds, they are able to be
307 selectively leached under the relatively mild pH conditions prevailing early in the reaction

308 process here. Slag dissolution in alkali-activated systems is often assumed to be congruent [35,
309 48-50], and this is consistent with the dissolution taking place rapidly under far-from-
310 equilibrium conditions where Si-O-(Si,Al) bonds can readily be broken. However, at a more
311 moderate pH and in the presence of carbonate, which is driving the extraction of calcium from
312 the slag glass, the Q⁰ sites would logically be prone to preferential release. This is observed in
313 the spectra in Figure 4A by the fact that the region from -65 to -70 ppm decreases significantly
314 in intensity within the first day of reaction. After this time, there is little additional change in
315 this part of the spectra, suggesting that the slag dissolution proceeds close to congruently
316 beyond this point.

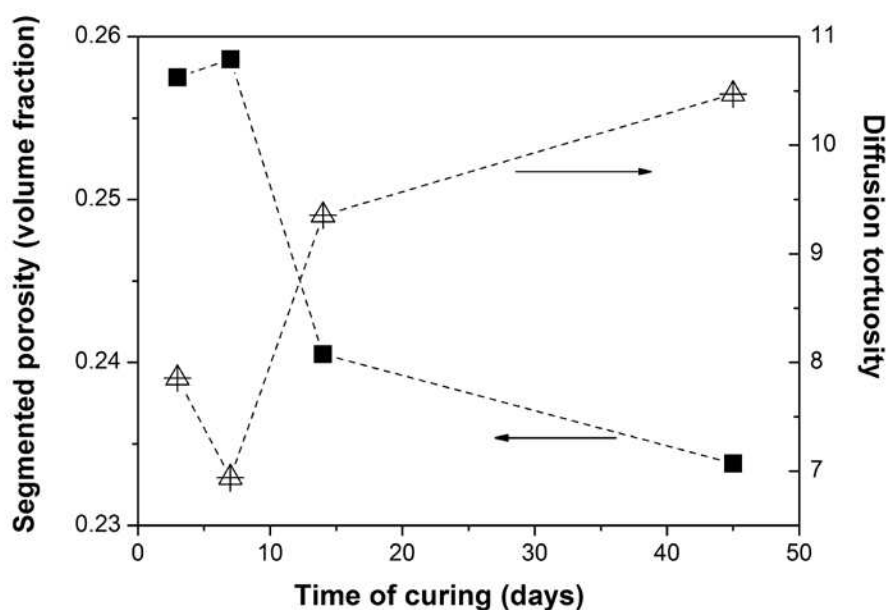
317
318 Three distinct types of aluminium environments, Al(IV) (52-80 ppm), Al(V) (30-40 ppm) and
319 Al(VI) (0-20 ppm) [51], are identified in all of the ²⁷Al MAS NMR spectra. Figure 4B shows
320 sharpening in the tetrahedral Al band after 7 d of curing compared with the unreacted slag,
321 along with the formation of a narrow peak at 74 ppm, whose intensity increases with curing
322 time. This band is assigned to the Al(IV) incorporated in bridging tetrahedra bonded to Q²(1Al)
323 sites in the C-A-S-H [39, 47]. After 28 days of curing, asymmetric broadening of the band at
324 68 ppm is observed, along with the formation of a low intensity shoulder at ~58 ppm, consistent
325 with the formation of Al-substituted tobermorites with low Ca/(Si+Al) ratio [39]. Small
326 contributions of the zeolite heulandite identified by XRD (Figure 3) are expected at around 63
327 ppm, [52], and the band at 62 ppm whose intensity seems to be higher at advanced times of
328 curing is consistent with this phase. At extended times of curing, the formation of a narrow
329 peak centred at 8.7 ppm is also observed. This peak corresponds to the hydrotalcite type phases,
330 and the increased intensity of this band over the time of curing is consistent with the XRD data
331 (Figure 3).

332

333 **3.5. X-ray microtomography (μCT)**

334 High resolution X-ray microtomography (μCT) has been proven to be a suitable technique for
335 the study of pore structure and tortuosity in alkali-activated binders [33] and in Portland cement
336 materials [53, 54], via segmentation of the samples into pore and solid regions to identify pore
337 geometry and tortuosity. The calculation of the porosity and tortuosity here follows the
338 methodology detailed in [33], and the results for samples of different ages are shown in Figure
339 5.

340



341
342 **Figure 5.** Segmented porosity and diffusion tortuosity of sodium carbonate-activated slag
343 binders as function of the time of curing. Estimated uncertainty is $\pm 3\%$ of the porosity (i.e.
344 around ± 0.005 in the porosity fractions plotted here), and ± 0.5 units in tortuosity.

345
346 The porosity values (Figure 5) decrease with increasing curing duration, and fall within a
347 similar range to the values published in [33] for sodium metasilicate-activated slag binders of
348 comparable mix design. The porosities at 14 and 45 days in the sodium carbonate-activated
349 specimens here are around 10% lower than the corresponding data for the silicate-activated
350 binders in [33], which were of similar mix designs. It is likely that the apparent increase in
351 porosity in the 7-day sample (and corresponding drop in tortuosity) actually falls within
352 experimental uncertainty for the expected monotonic behaviour; there is not a good
353 microstructural explanation for a temporary increase in porosity at this time.

354
355 The diffusion tortuosity values of these specimens are notably higher than the values measured
356 for silicate-activated slag or slag-fly ash blends in [33]. The highest tortuosity determined in
357 that study was for the sodium metasilicate-100% slag binder at 45 days, which had a tortuosity
358 of 8. The sodium carbonate-activated slag binder here exceeds that value by 14 days of age,
359 and reaches a value of more than 10 by 45 days. This may be important for long term durability,
360 because diffusion tortuosity is defined as the ratio of the rate of diffusion of a species in free
361 space to its rate of diffusion within the material. This means that the diffusion tortuosity can be
362 interpreted as being related to the resistance to transport through the material by diffusive

363 mechanisms, and is therefore a key factor controlling the service life of a reinforced concrete
364 element.

365

366 The decrease in porosity and increase in tortuosity as a function of curing duration is also
367 consistent with the results for slag-rich alkali-activated binders, where this trend is attributed
368 to the growth of C-S-H type binding products which incorporate and chemically bind water.
369 Such products are formed in the Na₂CO₃-activated binders after the initial consumption of
370 carbonate from the activator has taken place, the dissolved carbonate concentration is low, and
371 so the Ca²⁺ released by further slag dissolution is free to react with silicates instead.

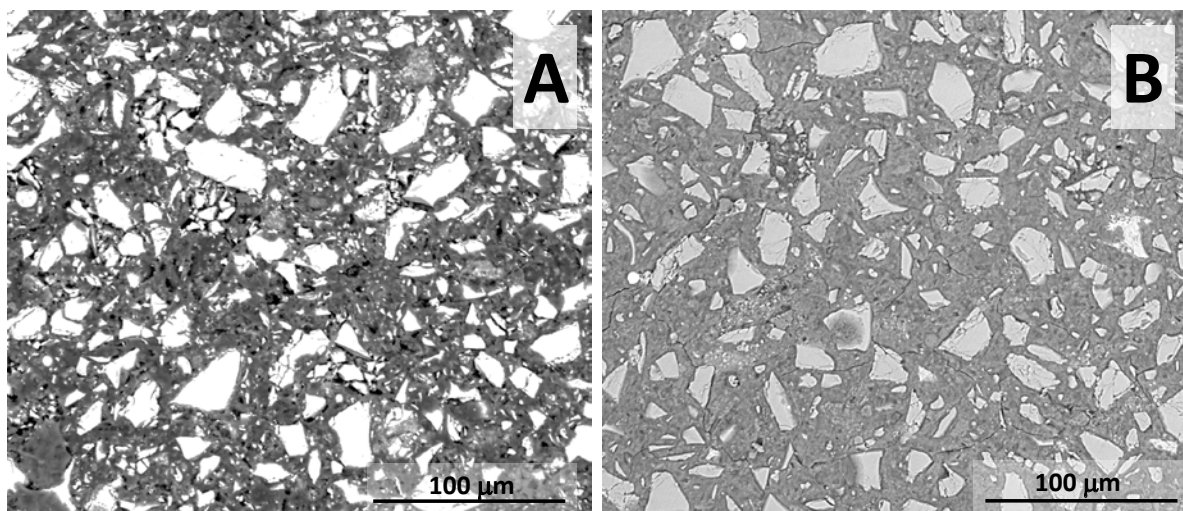
372

373

374 3.6. Scanning electron microscopy

375 A backscattered electron (BSE) image of 1-day cured Na₂CO₃ activated slag paste (Figure 6A)
376 shows a highly porous (black regions) and heterogeneous matrix (main grey region) with
377 embedded large angular particles (light grey) corresponding to unreacted slag. This
378 microstructure is consistent with the limited mechanical strength (Figure 1) and high porosity
379 (Figure 5) identified at early age. Conversely, after 56 days of curing (Figure 6B), the material
380 develops a cohesive and relatively homogeneous continuous matrix, in agreement with the
381 formation of space-filling reaction products such as C-A-S-H type gel, as previously identified
382 via XRD and NMR spectroscopy (Figures 3 and 4, respectively).

383

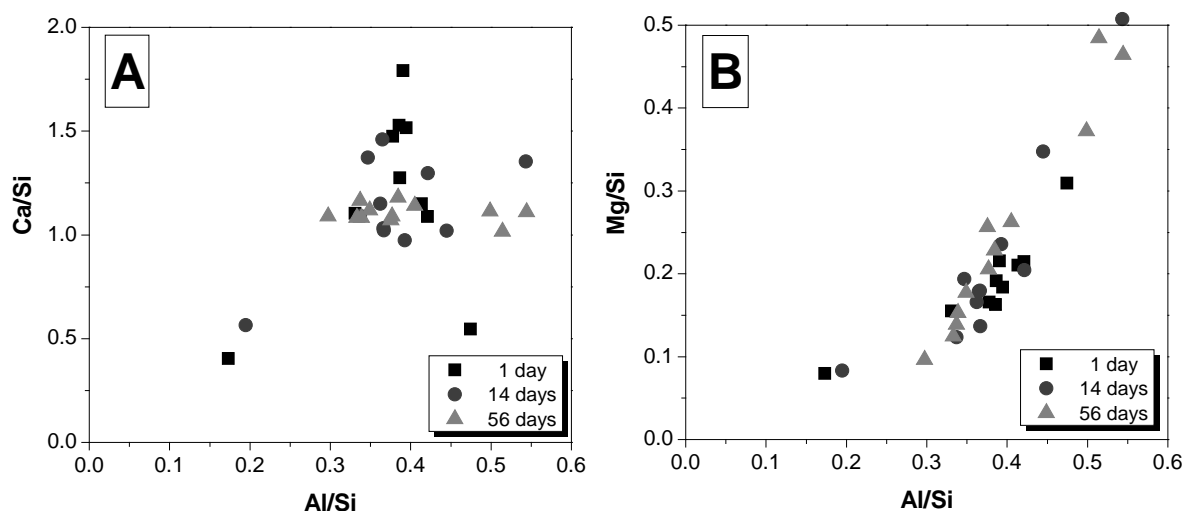


384

385 **Figure 6.** Backscattered electron images of alkali carbonate-activated slag binders after (A) 1
386 day and (B) 56 days of curing

387

388 EDX results for multiple points selected within the binder regions (i.e. excluding unreacted
389 precursor particles) over the time of curing are shown in Figure 7. The Ca/Si vs Al/Si plot
390 shows that the Al-substituted C-S-H type gel must be intimately intermixed with additional Al-
391 rich products, as the Al/Si ratio is very high for a pure chain-structured C-A-S-H type phase,
392 and is too high to show any notable degree of crosslinking [49]. This identification of additional
393 products is consistent with the identification of Al-rich zeolites and hydrotalcite-like layered
394 double hydroxides as secondary phases in these binders. The slope of the Mg/Si vs Al/Si plot
395 gives information regarding the overall composition of the layered double hydroxide phase,
396 which is seen to have an Mg/Al ratio of approximately 2 from these measurements. The data
397 appear to indicate a greater degree of consistency in Ca/Si ratio with increased curing time
398 (Figure 7A), as the gel is maturing and becoming more homogeneous as the binder develops.
399

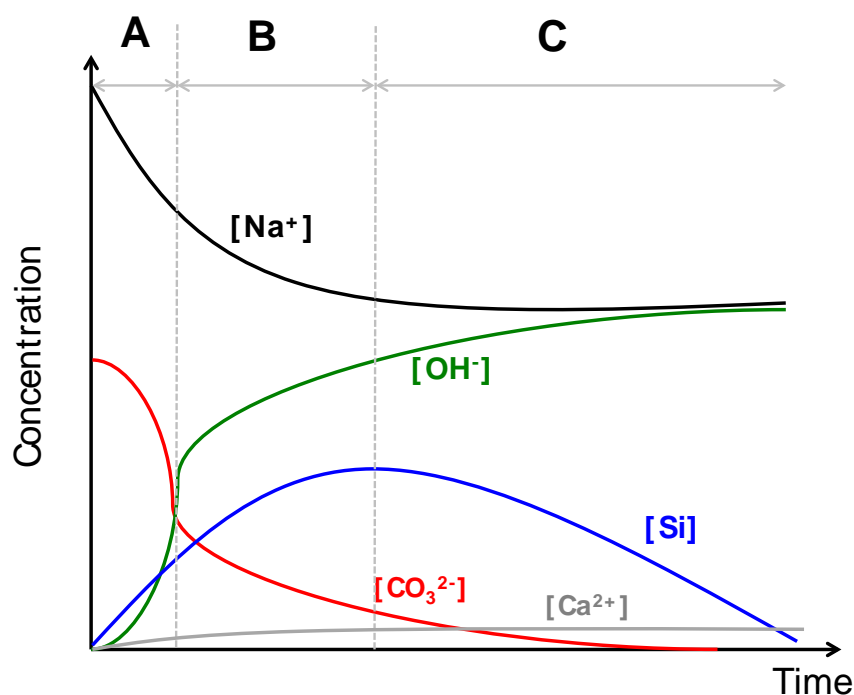


400
401 **Figure 7.** Atomic ratios (A) Ca/Si vs Al/Si and (B) Mg/Si vs Al/Si for bulk sodium carbonate
402 activated slag paste as function of curing duration
403

404 **3.7. Proposed conceptual description of the chemical mechanism of sodium** 405 **carbonate-activation reaction**

406
407 Based on the analytical results presented in this paper, and consistent with the known
408 mechanical and chemical evolution of alkali-carbonate activated slag binders up to very
409 extended ages [21], it is now possible to propose a detailed reaction mechanism for this reaction
410 process. Figure 8 describes, in a purely conceptual sense, the proposed evolution of the binder
411 chemistry according to three stages during which the changes in pore fluid chemistry are able
412 to influence and control the solid phase assemblage which is forming, as follows.

413



414

415 **Figure 8.** Proposed conceptual description of the pore solution chemistry within a sodium
416 carbonate-activated slag binder. The stages of the reaction process are described in detail in the
417 text; stage A is approximately the first day after mixing, stage B is the period up to
418 approximately 5 days corresponding to the induction period in isothermal calorimetry, and
419 stage C is the period beyond this, when calcium silicate-based binder phases are forming from
420 solution. The concentration axis scale is arbitrary, probably approximately 0-2 mol/L but
421 intended as indicative only.

422

423 **Stage A (~day 1):**

- 424 - Initial dissolution of slag, with heat release (pre-induction in calorimetry)
- 425 - Na_2CO_3 reacts with Ca^{2+} from slag to form gaylussite ($\text{Na}_2\text{Ca}(\text{CO}_3)_2 \cdot 5\text{H}_2\text{O}$)
- 426 - Si and Al from slag react with Na^+ to form zeolite A (Si/Al = 1.0)
- 427 - Dissolved OH^- and Si concentrations increasing

428

429 **Stage B (~days 1 to 5-7):**

- 430 - Induction period in calorimetry, dissolution of slag continuing
- 431 - Gaylussite converts to CaCO_3 and releases Na^+
- 432 - Zeolite phase Si/Al ratio seems to increase, with zeolite NaA replacement by
433 heulandite commencing

- 434 - Extra Al forms hydrotalcite with Mg^{2+} from slag
- 435 - Dissolved OH^- and Si concentrations still increasing

436

437 **Stage C (days 5-7 onwards):**

- 438 - Precipitation of bulk C-A-S-H gel, heat release in calorimetry
- 439 - Reduction of CO_3^{2-} concentration in solution, with a slight increase in Ca^{2+} (as its
- 440 solubility is no longer limited by saturation with respect to $CaCO_3$ polymorphs),
- 441 promotes precipitation of C-A-S-H instead of $CaCO_3$ and reduces porosity
- 442 - Dissolved Si concentration decreases with C-A-S-H formation; OH^- concentration
- 443 continues to increase and gives a highly alkaline pore solution (essentially NaOH) in
- 444 the hardened binder, which continues to react with the slag
- 445 - Mg^{2+} continues to form hydrotalcite with Al
- 446 - Zeolite formation slows notably after replacement of NaA by heulandite is complete

447

448 This reaction mechanism is therefore able to explain the chemistry of binder formation in the
449 alkali-activation of slag in a carbonate environment. The ongoing release of Ca, Si, Al and Mg
450 from the slag particles leads to the progressive reduction in porosity observed in Figure 6. The
451 relatively similar Ca/Si ratios between inner and outer products observed by Sakulich et al.
452 [25] in 20 month-old Na_2CO_3 -slag pastes are also consistent with a mechanism whereby the
453 slag is essentially reacting with an NaOH solution at greater ages, as there is no region which
454 is preferentially enriched with silica, the Mg and some of the Al are being consumed in
455 hydrotalcite formation, and the carbonate has already precipitated as $CaCO_3$.

456

457 From this basis, it is possible to draw implications regarding the design and optimisation of
458 binders based on alkali carbonate-activated slags. These are the potentially most cost-effective
459 and environmentally-friendly of all alkali-activated systems due to the much simpler and less
460 damaging process of production of Na_2CO_3 compared to the common industrial routes to
461 NaOH or sodium silicate production. They can generate excellent strength after 7 or 28 days
462 of curing, but the setting and hardening reactions of the systems studied here is not sufficiently
463 rapid for the materials to serve as a practical cementing binder system in general applications.
464 What seems to be required, to accelerate this process, would be a mechanism by which the
465 carbonate can be removed from solution at early age, leaving the slag to then react in a NaOH-
466 rich environment. There is therefore a need to develop such methods to manipulate the early
467 age pore solution chemistry of these materials, either through the use of solid or liquid

468 additives, to achieve this early-age binding of carbonate and thus elevated pH. The new
469 chemical understanding which has been developed in this paper will potentially hold the keys
470 to the next steps of development in this area, to make these binders into a viable system of
471 engineering materials for large-scale construction.

472

473

474 **4. Conclusions**

475

476 This paper has presented a detailed chemical and microstructural analysis of the mechanisms
477 of phase formation and strength development in sodium carbonate-activated slag binders.
478 These materials have been proposed as a low-CO₂ cementing binder system but tend to show
479 slow strength development, which has to some extent restricted the level of scientific analysis
480 which has been undertaken to date. However, the ability to understand and describe the
481 mechanisms by which these systems do react offers the scope for future developments and
482 optimisation of strength development performance, and so the results presented here are an
483 initial step towards enabling the further development and more widespread deployment of
484 materials based on this type of chemistry.

485

486 From analysis of the materials by diffractometry and spectroscopy, the phase evolution of these
487 materials, involving the initial precipitation of carbonates and zeolites (during the pre-induction
488 period as observed by calorimetry), with later development of C-A-S-H type phases (the
489 acceleration-deceleration period), has been elucidated. In the first days of reaction, the
490 carbonate supplied by the activator consumes essentially all of the calcium released by slag
491 dissolution; it is only when this carbonate is largely consumed that the formation of C-A-S-H
492 commences. The application of X-ray microtomography shows a significant ongoing decrease
493 in porosity at extended times of curing, resulting in a high-strength binder with a particularly
494 tortuous pore network, which is likely to be highly desirable for engineering applications if the
495 early-age strength evolution can be enhanced.

496

497

498

499 **Acknowledgements**

500

501 This work has been funded by the Australian Research Council, through a Linkage Project
502 cosponsored by Zeobond Pty Ltd, including partial funding through the Particulate Fluids
503 Processing Centre. We wish to thank Adam Kilcullen and David Brice for preparation of pastes
504 specimens, John Gehman for his assistance in NMR data collection and Volker Rose and
505 Xianghui Xiao for assistance in the data collection and processing on the 2BM instrument. Use
506 of the Advanced Photon Source was supported by the U.S. Department of Energy, Office of
507 Science, Office of Basic Energy Sciences, under Contract DE-AC02-06CH11357. The work
508 of JLP and SAB received funding from the European Research Council under the European
509 Union's Seventh Framework Programme (FP/2007-2013) / ERC Grant Agreement #335928
510 (GeopolyConc), and from the University of Sheffield.

511

512

513 **References**

514

- 515 1. van Deventer JSJ, Provis JL, Duxson P (2012) Technical and commercial progress in
516 the adoption of geopolymer cement. *Miner Eng* 29:89-104.
- 517 2. Provis JL, van Deventer JSJ, eds. *Alkali-Activated Materials: State-of-the-Art Report*,
518 *RILEM TC 224-AAM*. 2014, Springer/RILEM: Dordrecht.
- 519 3. Provis JL (2014) Green concrete or red herring? – the future of alkali-activated
520 materials. *Adv Appl Ceram*:in press.
- 521 4. Provis JL (2014) Geopolymers and other alkali activated materials - Why, how, and
522 what? *Mater Struct* 47(1):11-25.
- 523 5. Wang S-D, Pu X-C, Scrivener KL, Pratt PL (1995) Alkali-activated slag cement and
524 concrete: a review of properties and problems. *Adv Cem Res* 7(27):93-102.
- 525 6. Puertas F (1995) Cementos de escoria activados alcalinamente: situación actual y
526 perspectivas de futuro. *Mater Constr* 45(239):53-64.
- 527 7. Juenger MCG, Winnefeld F, Provis JL, Ideker J (2011) Advances in alternative
528 cementitious binders. *Cem Concr Res* 41(12):1232-1243.
- 529 8. Duxson P, Provis JL (2008) Designing precursors for geopolymer cements. *J Am*
530 *Ceram Soc* 91(12):3864-3869.
- 531 9. Shi C, Krivenko PV, Roy DM. *Alkali-Activated Cements and Concretes*, Abingdon,
532 UK: Taylor & Francis, 2006.
- 533 10. Provis JL, Bernal SA (2014) Geopolymers and related alkali-activated materials. *Annu*
534 *Rev Mater Res*:in press, DOI 10.1146/annurev-matsci-070813-113515.
- 535 11. Wang SD, Scrivener KL, Pratt PL (1994) Factors affecting the strength of alkali-
536 activated slag. *Cem Concr Res* 24(6):1033-1043.
- 537 12. Živica V (2007) Effects of type and dosage of alkaline activator and temperature on the
538 properties of alkali-activated slag mixtures. *Constr Build Mater* 21(7):1463-1469.
- 539 13. Fernández-Jiménez A, Puertas F (2003) Effect of activator mix on the hydration and
540 strength behaviour of alkali-activated slag cements. *Adv Cem Res* 15(3):129-136.
- 541 14. Shi C, On the state and role of alkalis during the activation of alkali-activated slag
542 cement, *Proceedings of the 11th International Congress on the Chemistry of Cement*,
543 Durban, South Africa, 2003.

- 544 15. Song S, Sohn D, Jennings HM, Mason TO (2000) Hydration of alkali-activated ground
545 granulated blast furnace slag. *J Mater Sci* 35:249-257.
- 546 16. Zhou H, Wu X, Xu Z, Tang M (1993) Kinetic study on hydration of alkali-activated
547 slag. *Cem Concr Res* 23(6):1253-1258.
- 548 17. Puertas F, Martínez-Ramírez S, Alonso S, Vázquez E (2000) Alkali-activated fly
549 ash/slag cement. Strength behaviour and hydration products. *Cem Concr Res* 30:1625-
550 1632.
- 551 18. Ben Haha M, Le Saout G, Winnefeld F, Lothenbach B (2011) Influence of activator
552 type on hydration kinetics, hydrate assemblage and microstructural development of
553 alkali activated blast-furnace slags. *Cem Concr Res* 41(3):301-310.
- 554 19. Kashani A, Provis JL, Qiao GG, van Deventer JSJ (2014) The interrelationship between
555 surface chemistry and rheology in alkali activated slag paste. *Constr Build*
556 *Mater*:submitted for publication.
- 557 20. Krivenko PV. Alkaline cements. In: Krivenko PV, ed. *Proceedings of the First*
558 *International Conference on Alkaline Cements and Concretes*. Kiev, Ukraine, VIPOL
559 Stock Company, 1994. 11-129.
- 560 21. Xu H, Provis JL, van Deventer JSJ, Krivenko PV (2008) Characterization of aged slag
561 concretes. *ACI Mater J* 105(2):131-139.
- 562 22. Provis JL, Duxson P, Kavalerova E, Krivenko PV, Pan Z, Puertas F, van Deventer JSJ.
563 Historical aspects and overview. In: Provis JL, van Deventer JSJ, *Alkali-Activated*
564 *Materials: State-of-the-Art Report*, RILEM TC 224-AAM, Springer/RILEM,
565 Dordrecht. 2014, p. 11-57.
- 566 23. Provis JL, Brice DG, Buchwald A, Duxson P, Kavalerova E, Krivenko PV, Shi C, van
567 Deventer JSJ, Wiercx JALM. Demonstration projects and applications in building and
568 civil infrastructure. In: Provis JL, van Deventer JSJ, *Alkali-Activated Materials: State-*
569 *of-the-Art Report*, RILEM TC 224-AAM, Springer/RILEM, Dordrecht. 2014, p. 309-
570 338.
- 571 24. Moseson AJ, Moseson DE, Barsoum MW (2012) High volume limestone alkali-
572 activated cement developed by design of experiment. *Cem Concr Compos* 34(3):328-
573 336.
- 574 25. Sakulich AR, Miller S, Barsoum MW (2010) Chemical and microstructural
575 characterization of 20-month-old alkali-activated slag cements. *J Am Ceram Soc*
576 93(6):1741-1748.
- 577 26. Moseson AJ. *Design and Implementation of Alkali Activated Cement for Sustainable*
578 *Development*. Ph.D. Thesis, Drexel University, 2011.
- 579 27. Bai Y, Collier N, Milestone N, Yang C (2011) The potential for using slags activated
580 with near neutral salts as immobilisation matrices for nuclear wastes containing reactive
581 metals. *J Nucl Mater* 413(3):183-192.
- 582 28. Bakharev T, Sanjayan JG, Cheng Y-B (1999) Alkali activation of Australian slag
583 cements. *Cem Concr Res* 29(1):113-120.
- 584 29. Fernández-Jiménez A, Puertas F (2001) Setting of alkali-activated slag cement.
585 Influence of activator nature. *Adv Cem Res* 13(3):115-121.
- 586 30. Duran Atiş C, Bilim C, Çelik Ö, Karahan O (2009) Influence of activator on the strength
587 and drying shrinkage of alkali-activated slag mortar. *Constr Build Mater* 23(1):548-
588 555.
- 589 31. Fernández-Jiménez A, Puertas F, Sobrados I, Sanz J (2003) Structure of calcium silicate
590 hydrates formed in alkaline-activated slag: Influence of the type of alkaline activator. *J*
591 *Am Ceram Soc* 86(8):1389-1394.
- 592 32. Wang YX, De Carlo F, Mancini DC, McNulty I, Tieman B, Bresnahan J, Foster I,
593 Insley J, Lane P, von Laszewski G, Kesselman C, Su MH, Thiebaut M (2001) A high-

- 594 throughput x-ray microtomography system at the Advanced Photon Source. *Rev Sci*
595 *Instrum* 72(4):2062-2068.
- 596 33. Provis JL, Myers RJ, White CE, Rose V, van Deventer JSJ (2012) X-ray
597 microtomography shows pore structure and tortuosity in alkali-activated binders. *Cem*
598 *Concr Res* 42(6):855-864.
- 599 34. Fernandez-Jimenez A, Puertas F, Arteaga A (1998) Determination of kinetic equations
600 of alkaline activation of blast furnace slag by means of calorimetric data. *J Thermal*
601 *Anal Calorim* 52(3):945-955.
- 602 35. Bernal SA, San Nicolas R, Myers RJ, Mejía de Gutiérrez R, Puertas F, van Deventer
603 JSJ, Provis JL (2014) MgO content of slag controls phase evolution and structural
604 changes induced by accelerated carbonation in alkali-activated binders. *Cem Concr Res*
605 57:33-43.
- 606 36. Ben Haha M, Lothenbach B, Le Saout G, Winnefeld F (2011) Influence of slag
607 chemistry on the hydration of alkali-activated blast-furnace slag -- Part I: Effect of
608 MgO. *Cem Concr Res* 41(9):955-963.
- 609 37. Bernal SA, Provis JL, Walkley B, San Nicolas R, Gehman J, Brice DG, Kilcullen A,
610 Duxson P, van Deventer JSJ (2013) Gel nanostructure in alkali-activated binders based
611 on slag and fly ash, and effects of accelerated carbonation. *Cem Concr Res* 53:127-144.
- 612 38. Bernal SA, Provis JL, Brice DG, Kilcullen A, Duxson P, van Deventer JSJ (2012)
613 Accelerated carbonation testing of alkali-activated binders significantly underestimate
614 the real service life: The role of the pore solution. *Cem Concr Res* 42(10):1317-1326.
- 615 39. Sun GK, Young JF, Kirkpatrick RJ (2006) The role of Al in C-S-H: NMR, XRD, and
616 compositional results for precipitated samples. *Cem Concr Res* 36(1):18-29.
- 617 40. Bernal SA, San Nicolas R, Provis JL, Mejía de Gutiérrez R, van Deventer JSJ (2014)
618 Natural carbonation of aged alkali-activated slag concretes. *Mater Struct*
619 DOI:10.1617/s11527-11013-10089-11522.
- 620 41. Escalante-Garcia J, Fuentes AF, Gorokhovskiy A, Fraire-Luna PE, Mendoza-Suarez G
621 (2003) Hydration products and reactivity of blast-furnace slag activated by various
622 alkalis. *J Am Ceram Soc* 86(12):2148-2153.
- 623 42. Bernal SA, Provis JL, Mejía de Gutiérrez R, van Deventer JSJ (2014) Accelerated
624 carbonation testing of alkali-activated slag/metakaolin blended concretes: effect of
625 exposure conditions. *Mater Struct*:in press.
- 626 43. Le Saoût G, Ben Haha M, Winnefeld F, Lothenbach B (2011) Hydration degree of
627 alkali-activated slags: A ^{29}Si NMR study. *J Am Ceram Soc* 94(12):4541-4547.
- 628 44. Benharrats N, Belbachir M, Legrand AP, D'Espinoze de la Caillerie J-B (2003) ^{29}Si and
629 ^{27}Al MAS NMR study of the zeolitization of kaolin by alkali leaching. *Clay Miner*
630 38(1):49-61.
- 631 45. Ward RL, McKague HL (1994) Clinoptilolite and heulandite structural differences as
632 revealed by multinuclear nuclear magnetic resonance spectroscopy. *J Phys Chem*
633 98(4):1232-1237.
- 634 46. Richardson IG, Brough AR, Brydson R, Groves GW, Dobson CM (1993) Location of
635 aluminum in substituted calcium silicate hydrate (C-S-H) gels as determined by ^{29}Si
636 and ^{27}Al NMR and EELS. *J Am Ceram Soc* 76(9):2285-2288.
- 637 47. Andersen MD, Jakobsen HJ, Skibsted J (2003) Incorporation of aluminum in the
638 calcium silicate hydrate (C-S-H) of hydrated Portland cements: A high-field ^{27}Al and
639 ^{29}Si MAS NMR investigation. *Inorg Chem* 42(7):2280-2287.
- 640 48. Ben Haha M, Lothenbach B, Le Saout G, Winnefeld F (2012) Influence of slag
641 chemistry on the hydration of alkali-activated blast-furnace slag -- Part II: Effect of
642 Al_2O_3 . *Cem Concr Res* 42(1):74-83.

- 643 49. Myers RJ, Bernal SA, San Nicolas R, Provis JL (2013) Generalized structural
644 description of calcium-sodium aluminosilicate hydrate gels: The crosslinked
645 substituted tobermorite model. *Langmuir* 29(17):5294-5306.
- 646 50. Bernal SA, Provis JL, Walkley B, San Nicolas R, Gehman JD, Brice DG, Kilcullen A,
647 Duxson P, van Deventer JSJ (2013) Gel nanostructure in alkali-activated binders based
648 on slag and fly ash, and effects of accelerated carbonation. *Cem Concr Res* 53:127-144.
- 649 51. Engelhardt G, Michel D. *High-Resolution Solid-State NMR of Silicates and Zeolites*,
650 Chichester: John Wiley & Sons, 1987.
- 651 52. Ward RL, McKague HL (1994) Clinoptilolite and heulandite structural differences as
652 revealed by multinuclear nuclear magnetic resonance spectroscopy. *J Phys Chem*
653 98(4):1232-1237.
- 654 53. Valentini L, Dalconi MC, Parisatto M, Cruciani G, Artioli G (2011) Towards three-
655 dimensional quantitative reconstruction of cement microstructure by X-ray diffraction
656 microtomography. *J Appl Cryst* 44:272-280.
- 657 54. Sugiyama T, Promentilla MAB, Hitomi T, Takeda N (2010) Application of synchrotron
658 microtomography for pore structure characterization of deteriorated cementitious
659 materials due to leaching. *Cem Concr Res* 40(8):1265-1270.
- 660
661